Graphene sheets wrapped carbon nanofibers as a highly conductive three-dimensional framework for perpendicularly anchoring of MoS$_2$: Advanced electrocatalysts for hydrogen evolution reaction

Huahao Gu[a], Yunpeng Huang[a], Lizeng Zuo[a], Wei Fan[b,*], Tianxi Liu[a,b,*]

[a] State Key Laboratory of Molecular Engineering of Polymers, Department of Macromolecular Science, Fudan University, 220 Handan Road, Shanghai 200433, PR China
[b] State Key Laboratory for Modification of Chemical Fibers and Polymer Materials, College of Materials Science and Engineering, Donghua University, 2999 North Renmin Road, Shanghai 201620, PR China

ARTICLE INFO

ABSTRACT

It is universally acknowledged that the development of high-efficiency Pt-free electrocatalysts for hydrogen evolution reaction (HER) is a challenging and demanding task nowadays. Herein, graphene wrapped carbon nanofiber @ molybdenum disulfide (GCNF@MoS$_2$) hybrids with hierarchical structure have been successfully prepared as HER electrocatalysts through the combination of electrospinning, solution soaking and solvothermal methods. The wrapping of few-layered graphene functions crucially as a "bridge" closely linking three-dimensional (3D) carbon nanofibers and electrocatalytically active MoS$_2$, providing a highly conductive pathway through the whole hybrids, thus facilitating the transport of electrons. Furthermore, carbon nanofibers acting as "spacers" between graphene layers can efficiently impede their restacking, thus giving full play to the superior electrical conductivity of graphene. Benefiting from the 3D network and template of GCNF, MoS$_2$ nanosheets can grow densely and perpendicularly on the fiber surface, therefore exposing catalytically active edges effectively. Owing to the synergistic effects among three components, the GCNF@MoS$_2$ hybrid exhibits remarkable electrocatalytic activity with a low onset potential of -0.08 V, a small Tafel slope of 49.6 mV per decade, a large current density (10.0 mA cm^{-2} at $\eta = 0.15$ V) as well as excellent stability. Apart from fabricating an efficient HER catalyst, this work also provides a practical strategy for designing hybrid materials with multi-functions for their potential applications in new energy field.

© 2016 Elsevier Ltd. All rights reserved.

1. Introduction

During the past decades, there has been a growing trend for the rapid consumption of exhaustible fossil fuels, which results in an urgent demand for sustainable and alternative energy resources and carriers [1]. It is well known that hydrogen is an ideal energy carrier with high gravimetric energy density [2]. Compared with the industrial method by steam reforming of natural gas, electro-catalytic water splitting provides a renewable and environmental-ly-friendly way to produce hydrogen [3]. The key point for hydrogen evolution reaction (HER, i.e., $2H^+ + 2e^- \rightarrow H_2$) depends on the electrocatalyst in cathode, which plays a vital role in determining the rate and efficiency of electrocatalytic reaction [4]. Theoretically, an excellent HER catalyst should be capable of making a balance between binding and releasing hydrogen atoms. To date, the most effective electrocatalysts for HER are platinum (Pt) and its alloys. They possess near-zero overpotential along with extremely high electrocatalytic rates, which can be attributed to their neither too strong nor too weak ability of combining with hydrogen atoms [5]. However, the extreme scarcity and high price of Pt-based materials have greatly limited their wide application. As a result, it is meaningful to search for alternative HER electrocatalysts with earth abundance and high efficiency.

Molybdenum disulfide (MoS$_2$) is a kind of two-dimensional transition metal chalcognide material, which has been tradition-ally used as catalysts for the hydrodesulfurization reaction as well as a solid lubricant [6]. Recent work shows that MoS$_2$ possesses great potential as a promising HER catalyst and its hydrogen binding energy is close to that of Pt [7,8]. Moreover, it has been

* Corresponding authors at: State Key Laboratory of Molecular Engineering of Polymers, Department of Macromolecular Science, Fudan University, 220 Handan Road, Shanghai, 200433, PR China.
E-mail addresses: weifan@dhu.edu.cn (W. Fan), txliu@fudan.edu.cn (T. Liu).

proved by both experimental [9] and computational [10] studies that the electrocatalytic property of MoS_2 originates from its co-ordinated sulfur edge sites, while the basal surfaces are catalytically inert. Based on this principle, defect-rich MoS_2 [11], edge-exposed MoS_2 nanoporous films [12] and nanoassemblies [13] have been explored. Besides increasing the density of exposed edge sites, the electrical conductivity of electrocatalysts is another key factor that should be taken into consideration. In this regard, constructing hybrids of MoS_2 with highly conductive templates is an efficient way to take full advantages of the excellent inner properties of HER active materials. Ideal matrices such as reduced graphene oxide [14], carbon nanotubes (CNTs) [15] and three-dimensional (3D) carbon aerogel [16] have been utilized to enhance the conductivity of the MoS_2-based electrocatalysts, as their strong chemical coupling can effectively improve the electrical contact from the templates to the active sites.

Among all carbon material, graphene, undoubtedly, is the best in terms of electrical conductivity. It is constructed by a single layer of sp^2 carbon atoms arranged hexagonally, and possesses unique properties, such as high theoretical surface area ($2630\,m^2\,g^{-1}$) and excellent intrinsic carrier mobility ($2,00,000\,cm^2\,V^{-1}\,S^{-1}$) [17]. However, due to the strong π-π stacking and van der waals interaction induced irreversible aggregation of graphene sheets, their outstanding properties can not be thoroughly exploited. In order to fully exert the potential of graphene nanosheets, many researchers try to introduce "spacers" between the graphene layers, such as CNTs [18] and polymer [19,20]. On the one hand, these "spacers" can effectively prevent the restacking of graphene nanosheets. On the other hand, the few-layered graphene nanosheets with high specific area can function as a connected framework to greatly enhance the electrical conductivity of the "spacers". As a result, hybridizing graphene with "spacers" is an efficient method to complement one another perfectly.

Besides two dimensional carbon matrices, one dimensional carbon nanofibers (CNFs) have also attracted a lot of attention, especially in the field of electrochemistry. As is well known, CNFs possess many outstanding characteristics such as large surface areas, excellent structural stability, good electrical conductivity as well as mechanical strengths and flexibility, thus making them promising candidates for electrode materials and catalyst substrates [21,22]. Electrospinning technique is a low-cost, scalable and versatile method to produce CNFs with tunable nanostructures [23]. As a result, a large number of studies based on electrospun carbon nanofibers in electrochemistry have been reported [24]. Although the electrical conductivity of CNFs is relatively high, it is still far away from graphene or CNTs. Therefore, it is meaningful to further enhance the conductivity of CNFs, taking full advantage of their excellent 3D network. Zhang et al. prepared the CNTs-loaded electrospun Si/CNF composite as anode for lithium battery, which presented larger capacity and superior rate performance compared to that without CNTs, due to its enhanced electrical conductivity and contact [25]. Moreover, metal oxides, e.g., Fe_2O_3 [26], $NiCo_2O_4$ [27], have been incorporated to CNF through a sol-gel process followed by annealing treatment, and functioned as additives to improve the conductivity or electrochemical activity of CNFs. Nevertheless, it is still a big challenge to homogeneously disperse the additives into the CNFs. Taking this into account, wrapping the conductive material onto the CNFs could be another good choice to uniformly enhance the conductivity of the whole material.

In this work, few-layered graphene sheets wrapped carbon nanofibers are employed as a highly conductive 3D framework for the anchoring of MoS_2, which has been facilely prepared through the combination of electrospinning, solution soaking and solvo-thermal methods. Thinnish graphene nanosheets bridge carbon nanofibers and MoS_2 closely, which greatly enhances the

conductivity of whole hybrid catalyst, thus facilitating the rapid transfer of electrons. Further, carbon nanofibers not only function as a 3D network with large surface area, but also act as the "spacers" between individual graphene sheets, taking full advantage of superb electrical conductivity of graphene. In addition, perpendicularly oriented MoS_2 nanosheets are densely coated onto the graphene wrapped carbon nanofibers through controlled morphology adjustment, consequently maximizing the effective number of exposed HER active edges to protons. Benefiting from their unique hierarchical structures, the designed hybrid materials exhibit excellent electrocatalytic performance, with an optimal onset potential as low as −0.08 V and a small Tafel slope of $49.6\,mV\,decade^{-1}$. Moreover, apart from fabricating an efficient HER catalyst, this work also provides a practical strategy for designing 3D framework of graphene wrapped carbon nanofibers, which have great potential in fully exerting the performance of electrochemically active materials.

2. Experimental

2.1. Reagents

Polyacrylonitrile (PAN, Mw = $150000\,g\,mol^{-1}$) was purchased from Sigma-Aldrich. Ammonium tetrathiomolybdate (($NH_4)_2MoS_4$) was purchased from J&K Chemical, with a purity of 99%. N,N-dimethylformamide (DMF) and ethanol were obtained from Shanghai Chemical Reagent Company. De-ionized water was used throughout all the experiments.

2.2. Preparation of electrospun GCNF@MoS$_2$ nanofiber membranes

The preparation process of GCNF@MoS_2 nanofiber membranes is schematically shown in Fig. 1. First, PAN nanofiber membranes were produced through a facile single-nozzle electrospinning technique. Briefly, 1.0 g PAN power was dissolved in 10 mL of DMF under vigorous stirring to form a homogenous solution, which was sucked into a 5 mL syringe with a stainless needle having an inner diameter of 0.5 mm. When a high voltage of 20 kV was applied to the system with a feeding rate of $0.25\,mm\,min^{-1}$, PAN nanofibers were produced and collected onto the aluminum drum collector with a distance of 17 cm away from the spinneret. The generated PAN nanofiber membranes were then pre-oxidized under 250 °C for 2 h with a heating rate of $1\,°C\,min^{-1}$ in an air atmosphere, thus obtaining o-PAN nanofiber membranes.

GO wrapped o-PAN nanofiber membranes were prepared via a facile solution soaking process. GO was synthesized from graphite powder by a modified Hummers method [28]. The o-PAN nanofiber membranes were soaked into $3\,mg\,mL^{-1}$ homogeneous GO aqueous dispersion for 12 h at room temperature without any stirring. The desired volume of GO dispersion was just required to completely immerse the membranes. Then, the samples were washed with de-ionized water and ethanol for several times to remove the unwrapped GO sheets, yielding the GO@o-PAN nanofiber membranes. After that, the generated GO@o-PAN nanofiber membranes were heated up to 800 °C at a rate of $5\,°C\,min^{-1}$ and held for 2 h in a nitrogen flow. During this thermal treatment, o-PAN was converted to carbon nanofibers, and simultaneously, GO was thermally reduced to graphene. The obtained carbon nanofiber membranes wrapped with graphene were named as GCNF.

Finally, different loading amounts of MoS_2 were decorated onto the GCNF through a solvothermal reaction. Briefly, a certain amount of ($NH_4)_2MoS_4$ (5 mg, 10 mg, 20 mg, or 40 mg) were added into 10 mL DMF, followed by sonicating to get a well-dispersed solution. The electrospun GCNF membrane ($1 \times 2\,cm^2$) was immersed into the above solution, followed by being transferred
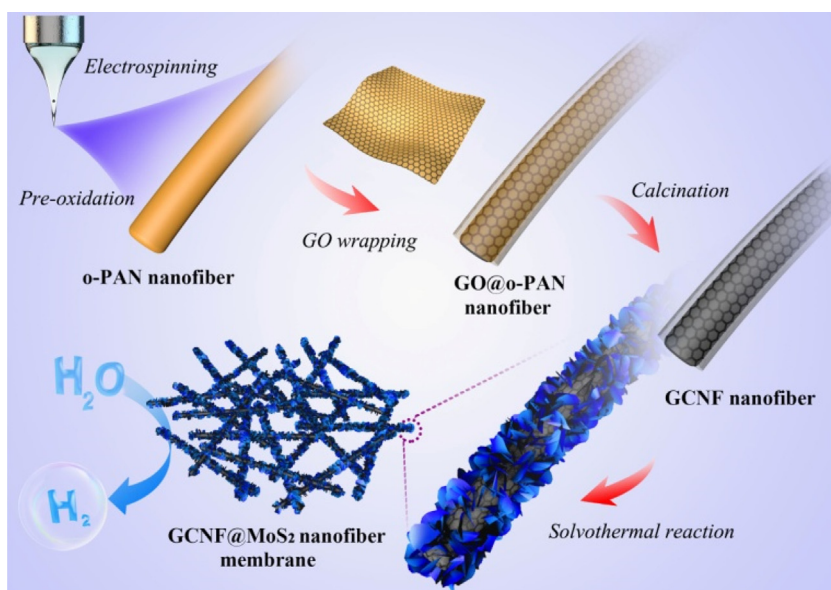
Fig 1. Schematic illustration of the preparation of GCNF@MoS$_2$ hybrids.

into a 40 mL Teflon-lined stainless steel autoclave to make a solvothermal reaction at 200 °C for 12 h. After the reaction system cooled down to room temperature, the hybrid membranes were cleaned with de-ionized water and ethanol and dried at 70 °C under vacuum. The hybrids with different loading amounts of MoS$_2$ were denoted as GCNF@MoS$_2$-5, GCNF@MoS$_2$-10, GCNF@MoS$_2$-20 and GCNF@MoS$_2$-40, respectively. For comparison, carbon nanofiber membranes without graphene were also prepared, labelled as CNF@MoS$_2$ hybrid membrane, with component ratio the same as GCNF@MoS$_2$-20 hybrid. In addition, pure GCNF fiber membrane was prepared via the above method without the addition of $(NH_4)_2MoS_4$ while pure MoS$_2$ was prepared without GCNF.

2.3. Characterization of GCNF@MoS$_2$ hybrids

Morphology of the products was observed using a field emission scanning electron microscope (FESEM, Ultra 55, Zeiss) at an acceleration voltage of 5 kV. Transmission electron microscopy (TEM) and high-solution transmission electron microscopy were performed under an acceleration voltage of 200 kV with a JEOL JEM2100 TEM. X-ray diffraction (XRD) experiments were conducted from $2\theta = 5°$ to $70°$ on an X'Pert Pro X-ray diffractometer with Cu Kα radiation ($\lambda = 0.1542$ nm) under a voltage of 40 kV and a current of 40 mA. Thermogravimetric analysis (Pyris 1 TGA) was performed under air flow from 100 to 700 °C at a heating rate of 20 °C min^{-1}. X-ray photoelectron spectroscopy (XPS) analyses were made with Thermo Scientific ESCALAB 250Xi using an Al Kα sources 1486.6 eV anode. All XPS spectra were corrected using C1 s line at 284.6 eV. The electrical conductivities of the samples were measured with a 4-point probes resistivity measurement system (RTS-8). The Brunauer-Emmett-Teller (BET) surface area was measured using a Belsorp-max surface area detecting instrument by N$_2$ physisorption at 77 K. The pore size distribution was derived from the desorption branch of isotherm using the Barrett-Joyner-Halenda (BJH) model.

2.4. Eelectrochemical studies

The electrochemical tests were performed in a standard three-electrode setup using a CHI 660D electrochemical workstation (Shanghai Chenhua Instrument Co., China), where a graphite rod was used as the counter electrode, a saturated calomel electrode (SCE) as the reference electrode and the modified GCE as the working electrode. Linear sweep voltammetry (LSV) was measured with a scan rate of 2 mV s^{-1} in 0.5 M H$_2$SO$_4$. The double-layer capacitance (C_{dl}) of catalyst can be calculated from the cyclic voltammograms in the region of 0-0.2 V vs. RHE. By plotting the Δj at 0.1 V vs. RHE against the scan rate, the slope is twice of C_{dl}. AC impedance measurements were carried out with frequencies ranging from 10^6 Hz to 10^{-2} Hz with an amplitude of 5 mV. All of the potentials were calibrated to a reversible hydrogen electrode (RHE).

3. Results and discussion

3.1. Morphology and structure of GCNF@MoS$_2$ hybrids

The wrapping process of graphene onto the CNF membranes is detected by FTIR and XRD. Fig. S1 shows the FTIR spectra of the PAN, o-PAN and GO@o-PAN fiber membranes. The characteristic vibrations of the chemical groups for PAN nanofibers are clearly presented in the spectra. The peaks located at 1452 and 2930 cm^{-1} refer to C-H bonds in alkyl groups while the peak at 2241 cm^{-1} corresponds to the C≡N groups. After the pre-oxidation process, there appears two absorption peaks at 1591 and 1371 cm^{-1} for o-PAN, along with an obvious reduction of intensity at the peaks of 2930 and 2241 cm^{-1}, which reflects the disappearance of linear structure induced by the cyclization and dehydrogenation reaction, thus forming an aromatic and heat-resistant structure [29]. The wrapping process of graphene oxide onto the surface of o-PAN nanofibers is driven by various interactions, which includes hydrogen bonding among functional groups, π-π stacking of sp^2-hybridized regions on the basal plane, as well as the van der waals forces between two components [30]. As for FTIR curve of GO@o-PAN hybrid nanofibers, a broad peak in the range of 3000–3500 cm^{-1}, along with another new peak at 1070 cm^{-1} emerges clearly after the wrapping of graphene oxide, which derives from stretching vibrations for hydroxyl groups and alkoxy groups of graphene oxide respectively. The wrapping process can also be confirmed by XRD patterns shown in Fig. 2. PAN nanofibers exhibit two strong diffraction peaks at $2\theta = 17.0°$ and $28.3°$. After pre-oxidation at 250 °C for 2 h, the intensity of the peak at $2\theta = 17.0°$ decreases apparently, indicating the crystalline regions in PAN
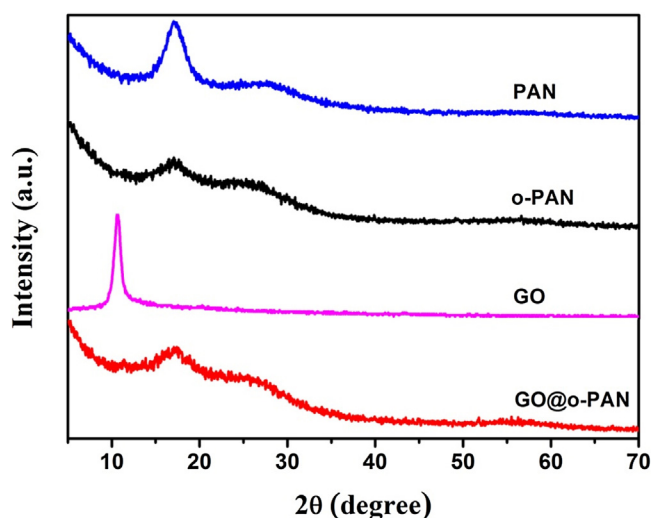
Fig. 2. XRD patterns of PAN, o-PAN, GO and GO@o-PAN hybrid.

linear macromolecules are gradually disappearing. Another broad peak shifts from $2\theta = 28.3°$ to $25.9°$, which reflects the formation of the conjugated ladder polymer structure along the chain axis for o-PAN nanofibers [31]. After the wrapping process, it is interesting to find that the characteristic peak of GO located at $2\theta = 11.0°$ almost disappears for GO@o-PAN hybrid. However, from the enlarged XRD pattern (red curve) in Fig. S2, the trace of the wrapped GO could still be slightly tracked (dashed square), which is different from that of pure o-PAN (black curve). The above phenomena not only further prove the wrapping process has been successfully realized, but also suggest only few-layered graphene oxide nanosheets are wrapped onto the carbon nanofibers without serious restacking,

which can make the best of the potential of the highly conductive graphene after calcination.

The morphology of CNF membranes and GCNF membranes are investigated by SEM and TEM images, as shown in Fig. 3 and Fig. S3. It can be clearly observed that after the wrapping of graphene, the original smooth surface of CNF becomes rough and wrinkled. Moreover, graphene wraps tightly onto the individual carbon nanofiber, which can greatly enhance the whole conductivity of the CNF membranes. As proved in Table S1, the electrical conductivity of GCNF membrane is measured to be $56.2\,\mathrm{S\,m^{-1}}$, which is almost three times of pure CNF membrane ($19.6\,\mathrm{S\,m^{-1}}$), fully giving prominence to the significance of wrapped graphene sheets. Consequently, GCNF not only inherits the 3D open network of the original CNF, but also possesses a highly conductive hierarchical nanostructure, making it an ideal substrate for the attachment of electrochemically active materials.

In the solvothermal process, different loading amounts of MoS_2 are decorated onto the surface of GCNF. From Fig. 4, it can be clearly seen that the overall morphology of GCNF@MoS_2 hybrids has significant changes with the increase of $(NH_4)_2MoS_4$ concentration. For GCNF@MoS_2-5 fibers, MoS_2 self-aggregates into nanospheres with different sizes, which scatter so sparsely onto the GCNF that some wrinkles derived from wrapped graphene could still be slightly discovered. With the increase of the amount of $(NH_4)_2MoS_4$ precursor, there is a tendency that the shape of MoS_2 changes from nanospheres to nanosheets, which is beneficial for the exposure of active edge sites for HER. For GCNF@MoS_2-10 hybrid, although a thin layer of MoS_2 nanosheets is horizontally covered onto the GCNF, the amount of attached MoS_2 nanosheets is far from enough in consideration of their size and density. By contrast, for GCNF@MoS_2-20 hybrid, it can be clearly observed that with the increase of nucleation sites, MoS_2 nanosheets are perpendicularly decorated onto the surface of GCNF network closely and uniformly. It is worth noted that such vertical layer
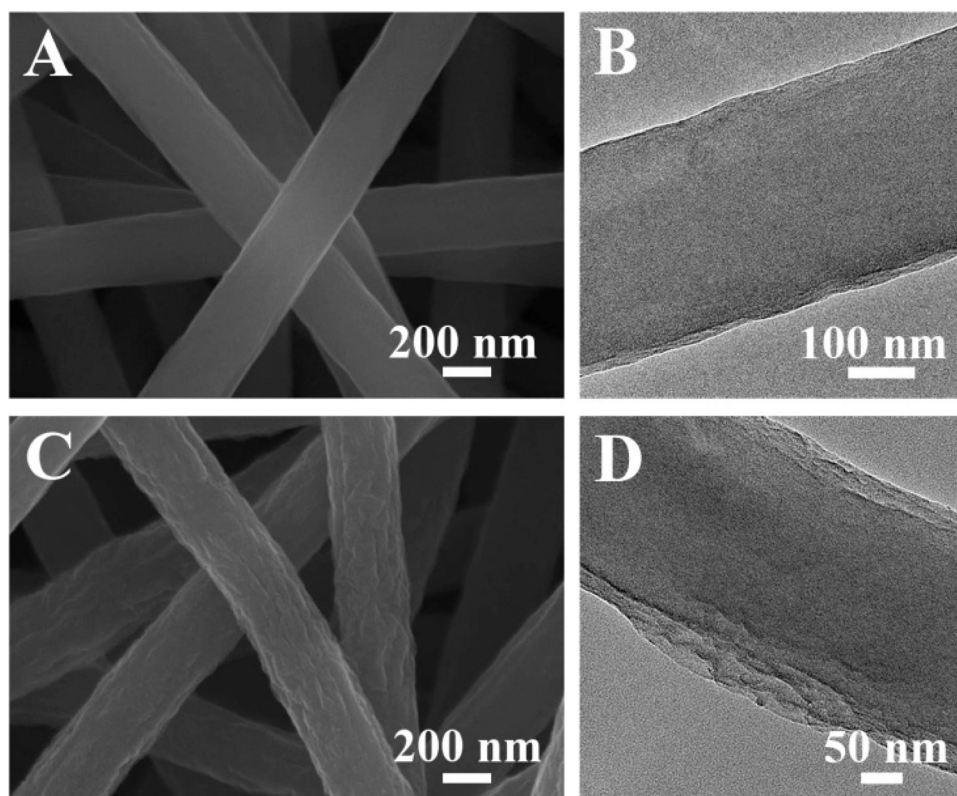
Fig. 3. FESEM (left) and TEM (right) images of (A, B) pristine CNF, and (C, D) GCNF.
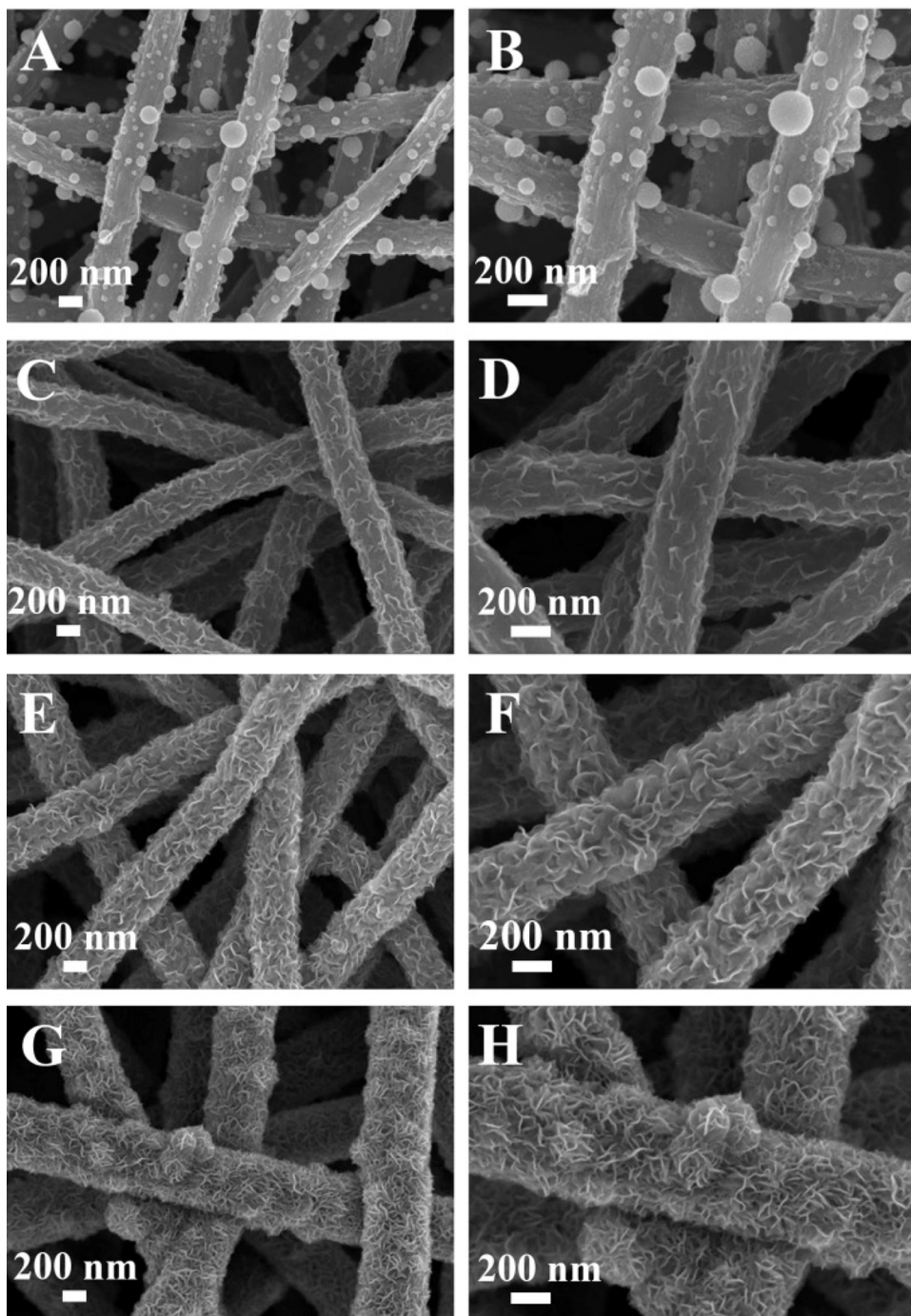
Fig. 4. FESEM images of (A, B) GCNF@MoS$_2$-5, (C, D) GCNF@MoS$_2$-10, (E, F) GCNF@MoS$_2$-20, (G, H) GCNF@MoS$_2$-40 hybrids at low (left) and high (right) magnifications.

orientation can efficiently expose more electrocatalytically active edges in comparison with that of GCNF@MoS$_2$-10 hybrid with horizontal growth direction. The EDS mapping images of GCNF@MoS$_2$-20 hybrid are shown in Fig. S4, the element distributions of Mo, S, and C verify the successful growth of MoS$_2$ onto the GCNF template. However, with excessive amount of (NH$_4$)$_2$MoS$_4$, MoS$_2$ nanosheets grow so densely that some aggregates inevitably appear, forming some packed bulges on the surface of the GCNF@MoS$_2$-40 hybrid fibers. For pure MoS$_2$ without GCNF template (Fig. S5), MoS$_2$ self-agglomerates into the hydrangea-like morphology, which greatly hinders the exposure of the catalytically active edge sites of MoS$_2$.

Furthermore, TEM image of GCNF@MoS$_2$-20 hybrid (Fig. 5) reveals that vertically oriented two-dimensional (2D) MoS$_2$ nanosheets are homogeneously anchored onto the one-dimensional (1D) graphene wrapped carbon nanofibers, forming a 3D hierarchical framework, which is in good agreement with the results of FESEM images. As a result, with MoS$_2$ nanosheets firmly anchored and evenly distributed on the surface of GCNF, GCNF@MoS$_2$-20 hybrid not only efficiently prevents the agglomeration of MoS$_2$ nanosheets, but also provides numerous active sites for rapid electrocatalytic reactions.

XPS spectra were investigated to confirm the compositions and chemical states of GCNF@MoS$_2$-20 hybrid. Fig. 6A clearly reveals
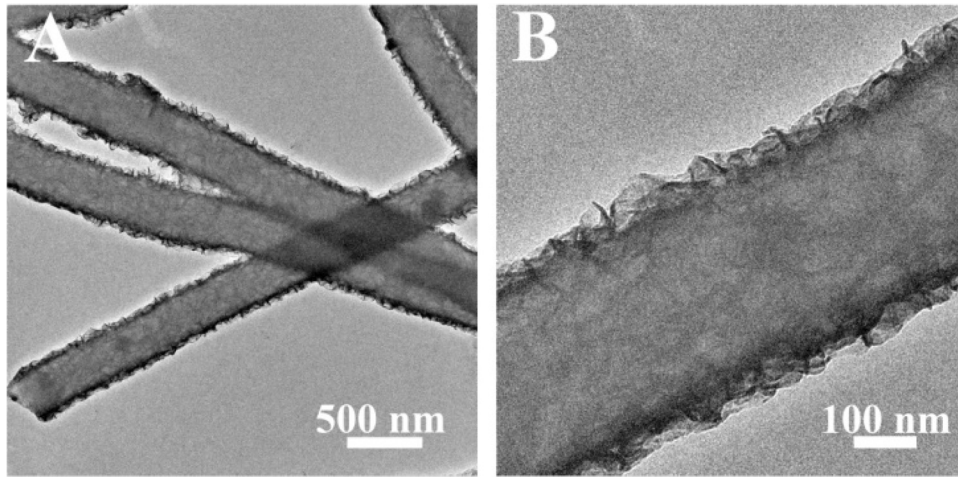
Fig. 5. TEM images of GCNF@MoS$_2$-20 hybrid at (A) low and (B) high magnifications.
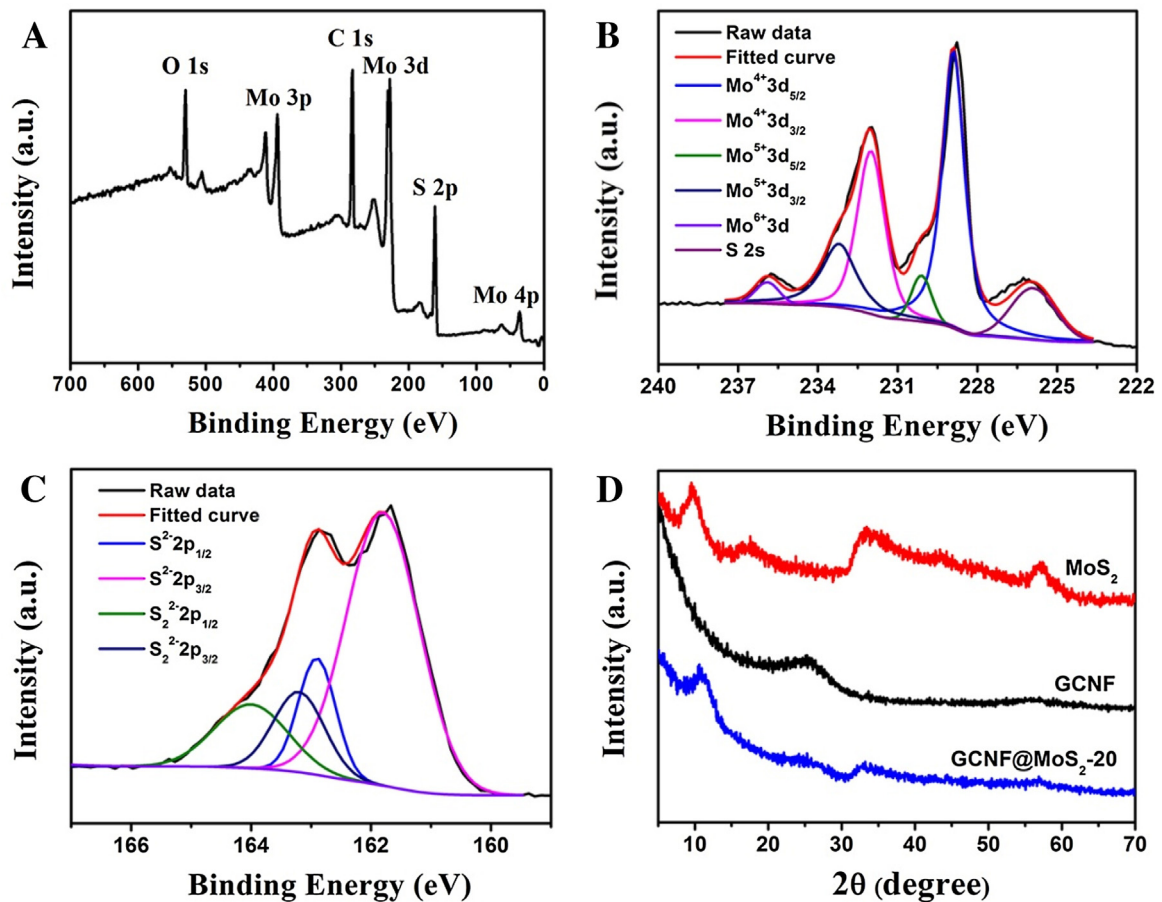
Fig. 6. XPS spectra of GCNF@MoS$_2$-20 hybrid: (A) survey spectrum, and high-resolution (B) Mo 3d, (C) S 2p spectrum. (D) XRD patterns of GCNF, MoS$_2$ and GCNF@MoS$_2$-20 hybrid.

the coexistence of C, Mo, S and O elements in the hybrid, without any detectable impurities. Fig. 6B and C depict high resolution Mo 3d and S 2p spectra, respectively. Two major peaks at 228.9 eV and 232.0 eV are presented in high resolution Mo 3d spectrum, corresponding to the binding energies of Mo 3d$_{5/2}$ and Mo 3d$_{3/2}$, characteristic of Mo^{4+} in MoS$_2$, indicating the dominance of Mo (IV) in the GCNF@MoS$_2$ hybrid [32]. The peaks centered at 230.1 eV and 233.2 eV can be assigned to Mo^{5+} ions, while the shoulder at 235.8 eV corresponds to higher +6 oxidation states, which may

result from the formation of MoO$_3$ induced by the inevitable surface exposure to air [33]. Moreover, a small peak at around 225.8 eV can be observed, which is ascribed to the S 2 s component in MoS$_2$. For the high resolution S 2p spectrum, the peaks located at 162.9 eV and 161.8 eV respectively refer to S 2p$_{1/2}$ and S 2p$_{3/2}$ orbits of divalent sulfide ions (S^{2-}) [34]. In addition, the S 2p$_{1/2}$ and S 2p$_{3/2}$ at 164.0 eV and 163.2 eV indicate the existence of bridging S$_2^{2-}$ [35]. For high resolution Mo 3d and S 2p spectra of pure MoS$_2$ (Fig. S6), it can be discovered that the peaks representing Mo^{4+} and

S^{2-} states occupy lower proportions compared with those of GCNF@MoS$_2$-20 hybrid, suggesting that MoS$_2$ can be prepared in higher purity with the support of GCNF template. XRD patterns were further used to prove the successful preparation of GCNF@MoS$_2$ hybrids, as shown in Fig. 6D. Different from that of GO@o-PAN, the pattern of GCNF displays a broad diffraction peak at $2\theta = 25.8°$, indicating graphene oxide wrapped o-PAN nanofibers have converted to graphene wrapped carbon nanofibers after calcination at 800 °C for 2 h. For pure MoS$_2$, two broad peaks at $2\theta = 32.8°, 57.3°$ can be well indexed to (100) and (110) diffraction planes of MoS$_2$, while two peaks at $2\theta = 9.6°, 18.6°$ indicate oxygen-incorporated MoS$_2$ ultrathin nanosheets, with similar phenomena reported in other literatures [36]. Furthermore, it can be seen that for GCNF@MoS$_2$-20 hybrid, some characteristic diffraction peaks of MoS$_2$ and GCNF could be found. All the above results strongly demonstrate the successful construction of GCNF@MoS$_2$ hybrids.

The loading percentage of MoS$_2$ in the GCNF@MoS$_2$ hybrids can be calculated from the TGA curves (Fig. S7). After being heated up to 700 °C in air, GCNF almost has no weight left, indicating its complete decomposition. Meanwhile, pure MoS$_2$ shows 16.7 wt% weight loss, indicating its transformation to molybdenum oxide. Therefore, the process of the weight loss for GCNF@MoS$_2$ hybrids combines the decomposition of GCNF with the transformation of MoS$_2$. From this aspect, the loading percentage of MoS$_2$ in the hybrids can be calculated to be 8.7 wt%, 20.6 wt%, 44.2 wt% and 63.6 wt% for GCNF@MoS$_2$-5, GCNF@MoS$_2$-10, GCNF@MoS$_2$-20 and GCNF@MoS$_2$-40 hybrids, respectively.

3.2. HER electrocatalytic activity of GCNF@MoS$_2$ hybrids

The electrocatalytic HER activities of GCNF@MoS$_2$ hybrids were investigated in 0.5 M H$_2$SO$_4$ solution with a three-electrode setup at a scan rate of 2 mV s^{-1}. Fig. 7 shows the LSV curves for GCNF@MoS$_2$ hybrids with different MoS$_2$ loading percentages. The criterion for the judgment of an outstanding HER catalyst lies in two key points. One is the low electrochemical overpotential (η), which is the difference between the applied and thermodynamic potentials of a given electrochemical reaction. Another one is the large electrochemical current density, which indicates the output of catalytically produced hydrogen. As a result, it can be clearly observed that among the GCNF@MoS$_2$ hybrids, GCNF@MoS$_2$-20 modified GCE exhibits the best HER catalytic performance, with apparent cathodic currents at the potential of −0.08 V, which is far small than those of the other GCNF@MoS$_2$ hybrids. This small onset
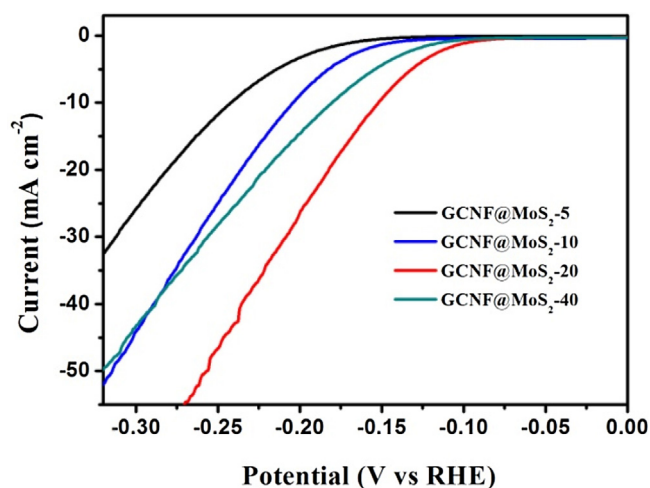
Fig. 7. LSV polarization curves for GCNF@MoS$_2$-5, GCNF@MoS$_2$-10, GCNF @MoS$_2$-20 and GCNF@MoS$_2$-40 hybrids modified GCE in N$_2$-purged 0.5 M H$_2$SO$_4$ solution.

overpotential of 0.08 mV indicates an excellent HER performance, which is superior to some previous reports, such as MoS$_2$/reduced GO paper (0.19 V) [37], MoS$_2$/carbon nanotube nanocomposite (0.09 V) [15] and defect-rich MoS$_2$ nanosheets (0.12 V) [11]. Moreover, GCNF@MoS$_2$-20 hybrid presents substantial current density (j) of 10.0 mA cm^{-2} at $\eta = 0.15$ V, comparing with 0.4 mA cm^{-2} for GCNF@MoS$_2$-5, 1.3 mA cm^{-2} for GCNF@MoS$_2$-10 and 4.5 mA cm^{-2} for GCNF@MoS$_2$-40. As is well known, the HER activity of MoS$_2$ arises from the sites located along the edges of MoS$_2$ layers, while the basal surfaces are catalytically inert. Therefore, it can be deduced that MoS$_2$ in nanosheet morphology can effectively expose more edge sites compared with that of nanosphere, which leads to the worst HER activity for GCNF@MoS$_2$-5 hybrid with the least MoS$_2$ loading amounts of 8.7 wt%. Although some horizontally oriented MoS$_2$ nanosheets exist in GCNF@MoS$_2$-10, the MoS$_2$ layer at such a loading content (20.6 wt%) and orientation could not make a full coverage of GCNF template (Fig. 4C and D), resulting in inadequate exposure and utilization of MoS$_2$ edge sites. In contrast, excessive coverage of MoS$_2$ nanosheets (63.6 wt%) in GCNF@MoS$_2$-40 hybrid hugely impedes the ion penetration and blocks the exposure of edge sites during the electrocatalytic process. Furthermore, due to the poor intrinsic conductivity of MoS$_2$ itself, the exceedingly thick layer of MoS$_2$ will result in the decrease of conductivity of the whole hybrid. BET analysis of nitrogen adsorption/desorption isotherms was further performed to make explanations of the differences in HER activities among the hybrids with different MoS$_2$ loading percentages. As shown in Fig. S8, the GCNF@MoS$_2$-20 hybrid displays a typical IV isotherm with the pore size distribution mainly centered at 3–4 nm, which is in the mesoporous range. More importantly, with the moderate loading amount of MoS$_2$ (44.2 wt%), the specific surface area of GCNF@MoS$_2$-20 hybrid is 19.4 m^2 g^{-1}, which is relatively larger than that of other products (Table S2). The high surface area along with the perpendicular growth direction guarantees the maximal exposure of electrocatalytically active edges, while the mesoporous hierarchical architecture is favorable for the easier accessibility of electrolyte and faster electron transfer, thus leading to its optimal HER performance. In a word, with the same growth template, the electrocatalytic activities of catalysts are greatly influenced by two important facts. One is the loading amount of electrocatalytically active material on template, such as MoS$_2$, either too low or too high amount can lead to inferior performance. The other is its morphology. It would be better to make full exposure of electroactive sites as much as possible, thus making utmost utilization of its excellence HER potential.

Further comparison of HER performance among pure GCNF, MoS$_2$, CNF@MoS$_2$-20, GCNF@MoS$_2$-20 hybrid and commercially available Pt/C catalyst is also investigated. As shown in Fig. 8, the Pt/C catalyst exhibits superb electrocatalytic performance, with a near zero onset potential and a large current density. Pure GCNF displays no catalytic activity with a horizontal line against the potential. Although pure MoS$_2$ exhibits unnegligible HER performance, the current density and onset potential are far inferior to those of CNF@MoS$_2$-20 and GCNF@MoS$_2$-20 hybrids, which results from lacking of a highly conductive template to prevent serious agglomeration of MoS$_2$. Furthermore, it is worth noting that CNF@MoS$_2$-20 hybrid exhibits inferior HER performance to GCNF@MoS$_2$-20 hybrid, no matter in the aspect of onset potential ($\eta = 0.10$ V) or current density ($j = 10.0$ mA cm^{-2} at $\eta = 0.20$ V). Evidently, the great difference of the HER performance between two hybrids is caused by the wrapping of graphene, which plays an important role of making a highly conductive "bridge" between the carbon nanofibers and MoS$_2$ nanosheets. The wrapped graphene can accelerate the transport of electrons during the electrocatalytic process, thus effectively compensating the insufficient electrical

A

B
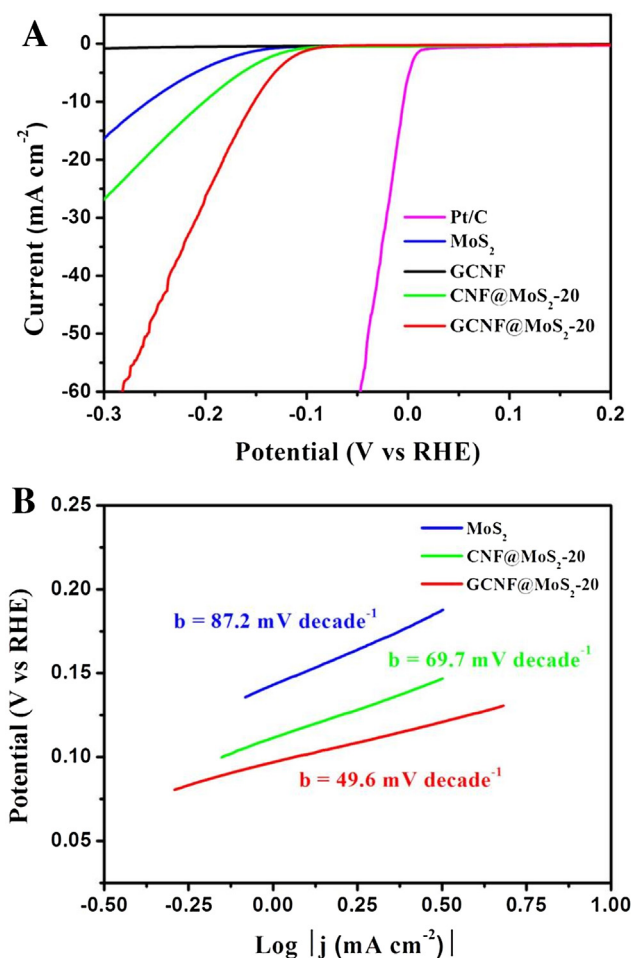
Fig. 8. (A) LSV polarization curves for different materials modified GCE in N_2-purged 0.5 M H_2SO_4 solution. (B) Tafel plots for pure MoS_2, CNF@MoS_2-20 and GCNF@MoS_2-20 hybrids modified GCE.

conductivity of CNFs. In addition, the electrochemical double-layer capacitances (C_{dl}) are also tested to confirm the effective electro-active surface area of catalysts via cyclic voltammetry measurements. It can be observed from Fig. S9 that GCNF@MoS_2-20 hybrid presents a larger C_{dl} of 60.5 mF cm^{-2} compared with that of CNF@MoS_2-20 hybrid, suggesting much more electrocatalytic active sites induced by the wrapped graphene "bridge", which makes great contributions to its better HER performance.

Tafel slope, an inherent property of the catalyst, is related to the reaction mechanism of a catalyst and determined by the rate-limiting step of the HER [5]. Tafel plots derived from the polarization curves of MoS_2, CNF@MoS_2-20 and GCNF@MoS_2-20 hybrids are shown in Fig. 8B. The linear portions of the Tafel plots are well fitted to the Tafel equation ($\eta = b\log(j) + a$, where η is the overpotential, j is the current density, and b is the Tafel slope), yielding Tafel slopes of 87.2 mV decade^{-1}, 69.7 mV decade^{-1} and 49.6 mV decade^{-1} for pure MoS_2, CNF@MoS_2-20 and GCNF@MoS_2-20 hybrids, respectively. The remarkably improved HER activities presented by the hybrids compared with pure MoS_2 suggest less activation energy for electrocatalytic performance, which can be ascribed to the confined growth of MoS_2 naosheets onto the template so that perpendicularly oriented, uniformly distributed and thereby edge-rich morphologies are formed for the CNF@MoS_2 and GCNF@MoS_2 hybrids. In addition, it should be highlighted that the Tafel slope of GCNF@MoS_2-20 hybrid is lower than that of

CNF@MoS_2-20 hybrid, demonstrating the higher hydrogen generation efficiency. The optimal HER performance of the GCNF@MoS_2-20 hybrid can be elucidated by the strong chemical coupling and electronic contact among the CNF, graphene and MoS_2, thus generating the synergistic effects on the hybrid structures. The electrospun CNF membrane makes a fundamental function to provide a growth template for MoS_2 nanosheets. The wrapping of few-layered graphene greatly enhances the conductivity of CNF matrix, thus efficiently promoting the electron transport during HER process, while the wrapping of graphene onto the CNFs further prevents the restacking or agglomeration of graphene nanosheets, exerting their outstanding electrical conductivity to the best. Furthermore, due to the strong interfacial interactions between graphene and CNFs, graphene wraps so intimately and uniformly onto the surface of CNFs that MoS_2 nanosheets anchor directly onto highly conductive graphene, which gives full play to the excellent HER potential of MoS_2. Besides, thanks to the template with 3D network, MoS_2 is confined to grow into the morphology of vertically oriented small nanosheets, which fully exposes its electrocatalytically active edge sites. These coordinated impacts lead to the distinctive performance of GCNF@MoS_2-20 hybrid, whose Tafel slope is lower than those of previously reported results, such as MoS_2/SnO_2 composite (59 mV decade^{-1}) [38], oxygen-incorporated MoS_2/graphene (51 mV decade^{-1}) [39], and carbon paper loaded MoS_2 (120 mV decade^{-1}) [40]. According to the classic theory on the mechanism of hydrogen evolution, the HER reaction may proceed via the following three possible reaction steps in acidic media.

Electrochemical hydrogen adsorption step (Volmer reaction):

$$H_3O^+ + e^- \rightarrow H_{ads} + H_2O \ (b \approx 120 \ mV) \tag{1}$$
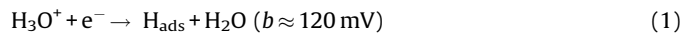
Electrochemical desorption step (Heyrovsky reaction):

$$H_{ads} + H_3O^+ + e^- \rightarrow H_2 + H_2O \ (b \approx 40 \ mV) \tag{2}$$

Chemical desorption step (Tafel step):

$$H_{ads} + H_{ads} \rightarrow H_2 \ (b \approx 30 \ mV) \tag{3}$$

As a result, the Tafel slope of 49.6 mV decade^{-1} for GCNF@MoS_2-20 hybrid suggests that HER activities take place via a rapid Volmer reaction, followed by a rate-limiting Heyrovsky reaction [41].

The HER stability of the electrode material is another vital criterion for an excellent electrocatalyst. As shown in Fig. 9A, the durability of GCNF@MoS_2-20 hybrid is investigated via carrying out continuous electrocatalytic HER performance at a constant overpotential of 0.17 V. It can be observed that the current density exhibits only a slight attenuation of less than 18.7% after cycling for 36000 seconds, revealing the long-term stability of GCNF@MoS_2-20 electrocatalyst, which can be ascribed to the firm combination among CNF, graphene and MoS_2 nanosheets. The enlarged inset in Fig. 9A further illustrates the alternate accumulation and release processes of produced H_2 (g) bubbles which occur fiercely on the surface of the electrode material, indicating the rapid depletion of H^+ in electrolyte, which may result in the degradation in current density. To make a better understanding of its stability, the morphology and structure of GCNF@MoS_2-20 hybrid after cycling test are also characterized delicately. As shown in Fig. 9B, it can be clearly discovered that MoS_2 nanosheets are still uniformly attached on the GCNF template despite a little decrease in the coverage density (see Fig. 4F for the morphology before cycling test), which may be due to the inevitable partial drop of MoS_2 nanosheets from the substrate during the violent hydrogen evolution process, thus leading to the decline in electrocatalytic performance. In addition, the XRD pattern of GCNF@MoS_2 hybrid (Fig. 9C) presents no significant changes compared with that
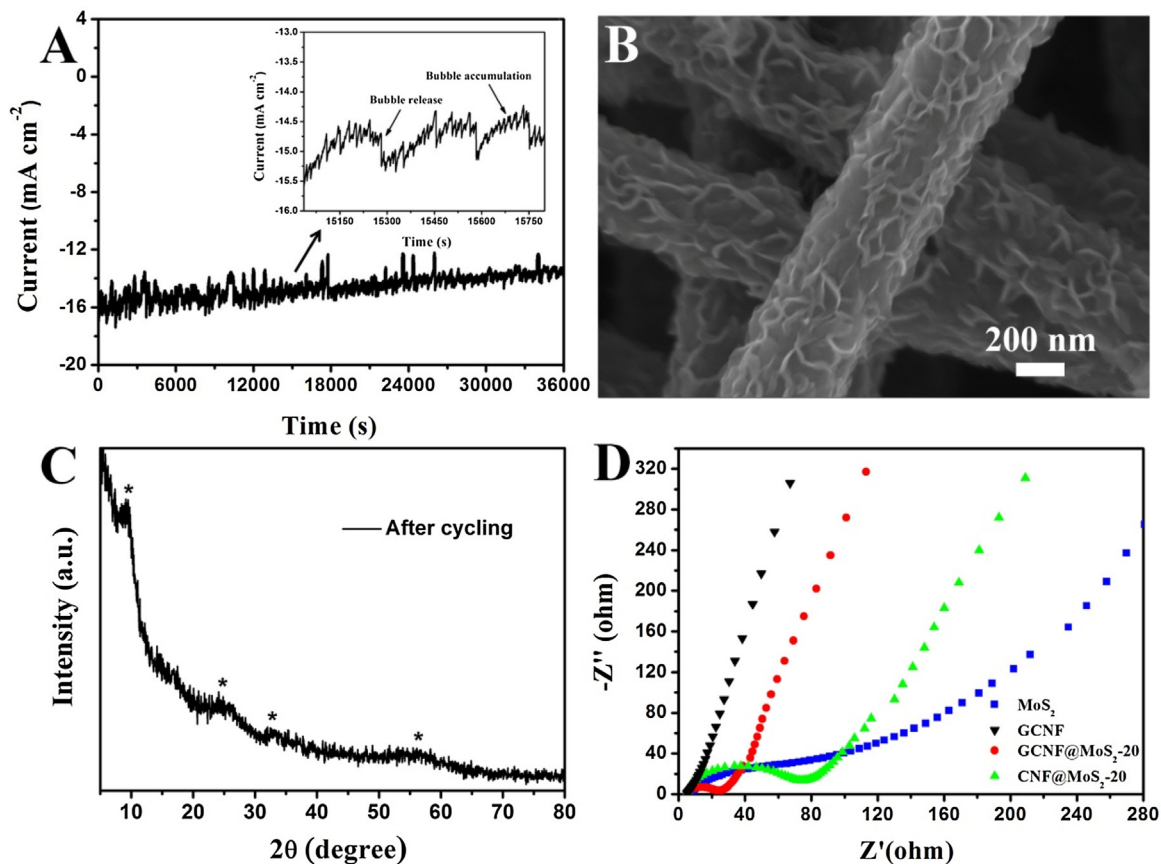
Fig. 9. (A) Time dependence of the current density for GCNF@MoS$_2$-20 modified GCE recorded at −0.17 V versus RHE. The inset is its enlarged curve from 15036 s to 15800s. (B) FESEM image of GCNF@MoS$_2$-20 hybrid after cycling test. (C) XRD pattern of GCNF@MoS$_2$-20 hybrid after cycling test. (D) Nyquist plots for GCNF, MoS$_2$, CNF@MoS$_2$-20 and GCNF@MoS$_2$-20 modified GCE.

before stability test (Fig. 6D), suggesting its good structure integrity. Electrochemical impedance spectroscopy (EIS) tests are also conducted to evaluate the electrochemical performance during the HER process. The Nyquist plots of GCNF, MoS$_2$, CNF@MoS$_2$-20 and GCNF@MoS$_2$-20 modified GCE are displayed in Fig. 9D. R_{ct} represents the charge transfer resistance, which corresponds to the semicircle of Nyquist plots, while R_s reveals the solution resistance, which is deduced from the *x*-intercept of Nyquist plots. It can be observed from Fig. 9D that all materials exhibit similar values for R_s, indicating the close contact between the electrocatalysts and the electrodes, as well as the good wettability between the electrolyte and the electrocatalysts. However, there are notable differences in R_{ct} among different HER catalysts. For GCNF, its Nyquist plot presents a nearly straight line without conspicuous semicircle in the high frequency region, revealing the ultralow charge transfer resistance during electrocatalytic process. Moreover, it can be easily found that GCNF@MoS$_2$-20 hybrid shows a much smaller R_{ct}, compared with that of CNF@MoS$_2$-20 hybrid, which again gives prominence to the important function of graphene wrapping. This highly conductive "bridge" is competent for facilitating the electron transport for the GCNF@MoS$_2$-20 electrocatalyst, which can also be speculated from the slope of Nyquist plots in the low frequency region. The steeper the line is, the faster the charge transfers. The slope of the linear part for GCNF@MoS$_2$-20 hybrid is much higher than that of CNF@MoS$_2$-20 hybrid, further confirming the decreased electrocatalytic resistance due to the wrapping of graphene. As for pure MoS$_2$, it exhibits a long arc in the high frequency region and a relatively flat curve in the low frequency region, suggesting its poor

electroactivity in charge transport compared with the hybrid materials, which results from the lack of an efficient template with high conductivity.

4. Conclusions

In summary, graphene wrapped carbon nanofibers have been utilized as an effective substrate for the growth of MoS$_2$ nanosheets, thus obtaining GCNF@MoS$_2$ hybrids for the application of HER electrocatalysts. This heterostructure is characterized by the wrapping of graphene, which functions as a highly conductive "bridge" connecting 3D interlacing carbon nanofibers and electrocatalytically active MoS$_2$ nanosheets compactly. Meanwhile, carbon nanofibers play an important role of "spacers" to prevent the restacking of graphene sheets. This synergistic effect makes GCNF an ideal substrate for the growth of electrochemically active materials owing to its high conductivity and large surface area, thus greatly accelerating the electron transport through the whole hybrid materials. As a result, the rationally designed GCNF@MoS$_2$ hybrid presents excellent HER activity with a low onset potential of −0.08 V, a small Tafel slope of 49.6 mV decade^{-1} and a large current density (10.0 mA cm^{-2} at η = 0.15 V), making them promising candidates for Pt-free electrocatalysts in hydrogen production.

Appendix A. Supplementary data

Supplementary data associated with this article can be found, in the online version, at http://dx.doi.org/10.1016/j.electacta.2016.10.015.

References

[1] M. Titirici, R.J. White, N. Brun, V.L. Budarin, D.S. Su, F. Del Monte, J.H. Clark, M.J. MacLachlan, Sustainable carbon materials, Chem. Soc. Rev. 44 (2015) 250–290.

[2] N. Muradov, T. Veziroglu, Green path from fossil-based to hydrogen economy: An overview of carbon-neutral technologies, Int. J. Hydrogen Energy 33 (2008) 6804–6839.

[3] M. Zeng, Y.G. Li, Recent advances in heterogeneous electrocatalysts for the hydrogen evolution reaction, J. Mater. Chem. A 3 (2015) 14942–14962.

[4] C.G. Morales-Guio, L.A. Stern, X.L. Hu, Nanostructured hydrotreating catalysts for electrochemical hydrogen evolution, Chem. Soc. Rev. 43 (2014) 6555–6569.

[5] Y. Yan, B.Y. Xia, Z.C. Xu, X. Wang, Recent development of molybdenum sulfides as advanced electrocatalysts for hydrogen evolution reaction, ACS Catal. 4 (2014) 1693–1705.

[6] D. Merki, X.L. Hu, Recent developments of molybdenum and tungsten sulfides as hydrogen evolution catalysts, Energy Environ. Sci. 4 (2011) 3878–3888.

[7] C.G. Morales-Guio, X.L. Hu, Amorphous molybdenum sulfides as hydrogen evolution catalysts, Acc. Chem. Res. 47 (2014) 2671–2681.

[8] A.B. Laursen, S. Kegnaes, S. Dahl, I. Chorkendorff, Molybdenum sulfides-efficient and viable materials for electro- and photoelectrocatalytic hydrogen evolution, Energy Environ. Sci. 5 (2012) 5577–5591.

[9] T.F. Jaramillo, K.P. Jørgensen, J. Bonde, J.H. Nielsen, S. Horch, I. Chorkendorff, Identification of active edge sites for electrochemical H_2 evolution from MoS_2 nanocatalysts, Science 317 (2007) 100–102.

[10] B. Hinnemann, P.G. Moses, J. Bonde, K.P. Jørgensen, J.H. Nielsen, S. Horch, I. Chorkendorff, J.K. Nørskov, Biomimetic hydrogen evolution: MoS_2 nanoparticles as catalyst for hydrogen evolution, J. Am. Chem. Soc. 127 (2005) 5308–5309.

[11] J.F. Xie, H. Zhang, S. Li, R.X. Wang, X. Sun, M. Zhou, J.F. Zhou, X.W. Lou, Y. Xie, Defect-rich MoS_2 ultrathin nanosheets with additional active edge sites for enhanced electrocatalytic hydrogen evolution, Adv. Mater. 25 (2013) 5807–5813.

[12] Y. Yang, H.L. Fei, G.D. Ruan, C.S. Xiang, J.M. Tour, Edge-oriented MoS_2 nanoporous films as flexible electrodes for hydrogen evolution reactions and supercapacitor devices, Adv. Mater. 26 (2014) 8163–8168.

[13] D.Y. Chung, S.K. Park, Y.H. Chung, S.H. Yu, D.H. Lim, N. Jung, H.C. Ham, H.Y. Park, Y.Z. Piao, S.J. Yoo, Y.E. Sung, Edge-exposed MoS_2 nano-assembled structures as efficient electrocatalysts for hydrogen evolution reaction, Nanoscale 6 (2014) 2131–2136.

[14] Y.G. Li, H.L. Wang, L.M. Xie, Y.Y. Liang, G.S. Hong, H.J. Dai, MoS_2 nanoparticles grown on graphene: An advanced catalyst for the hydrogen evolution reaction, J. Am. Chem. Soc. 133 (2011) 7296–7299.

[15] Y. Yan, X.M. Ge, Z.L. Liu, J.Y. Wang, J.M. Lee, X. Wang, Facile synthesis of low crystalline MoS_2 nanosheet-coated CNTs for enhanced hydrogen evolution reaction, Nanoscale 5 (2013) 7768–7771.

[16] Y.F. Zhang, L.Z. Zuo, Y.P. Huang, L.S. Zhang, F.L. Lai, W. Fan, T.X. Liu, In-situ growth of few-layered MoS_2 nanosheets on highly porous carbon aerogel as advanced electrocatalysts for hydrogen evolution reaction, ACS Sustainable Chem. Eng. 3 (2015) 3140–3148.

[17] C.H. Xu, B.H. Xu, Y. Gu, Z.G. Xiong, J. Sun, X.S. Zhao, Graphene-based electrodes for electrochemical energy storage, Energy Environ. Sci. 6 (2013) 1388–1414.

[18] L.S. Zhang, Y.P. Huang, Y.F. Zhang, W. Fan, T.X. Liu, Three-dimensional nanoporous graphene-carbon nanotube hybrid frameworks for confinement of SnS_2 nanosheets: Flexible and binder-Free papers with highly reversible lithium storage, ACS Appl. Mater. Interfaces 7 (2015) 27823–27830.

[19] C. Zhang, T.X. Liu, A review on hybridization modification of graphene and its polymer nanocomposites, Chin. Sci. Bull. 57 (2012) 3010–3021.

[20] G.Q. Tang, Z.G. Jiang, X.F. Li, H.B. Zhang, Z.Z. Yu, Simultaneous functionalization and reduction of graphene oxide with polyetheramine and its electrically conductive epoxy nanocomposites, Chin. J. Polym. Sci. 32 (2014) 975–985.

[21] Y.E. Miao, Y.P. Huang, L.S. Zhang, W. Fan, F.L. Lai, T.X. Liu, Electrospun porous carbon nanofiber@MoS_2 core/sheath fiber membranes as highly flexible and binder-free anodes for lithium-ion batteries, Nanoscale 7 (2015) 11093–11101.

[22] Q.W. Ding, M.K. Liu, Y.E. Miao, Y.P. Huang, T.X. Liu, Electrospun nickel-decorated carbon nanofiber membranes as efficient electrocatalysts for hydrogen evolution reaction, Electrochim. Acta 159 (2015) 1–7.

[23] B. Zhang, F.Y. Kang, J.M. Tarascon, J.K. Kim, Recent advances in electrospun carbon nanofibers and their application in electrochemical energy storage, Prog. Mater. Sci. 76 (2016) 319–380.

[24] Z.X. Dong, S.J. Kennedy, Y.Q. Wu, Electrospinning materials for energy-related applications and devices, J. Power Sources 196 (2011) 4886–4904.

[25] Y. Li, G.J. Xu, L.G. Xue, S. Zhang, Y.F. Yao, Y. Lu, O. Toprakci, X.W. Zhang, Enhanced rate capability by employing carbon Nanotube-Loaded electrospun Si/C composite nanofibers as binder-free anodes, J. Electrochem. Soc. 160 (2013) A528–A534.

[26] G. Binitha, M.S. Soumya, A.A. Madhavan, P. Praveen, A. Balakrishnan, K.R.V. Subramanian, M.V. Reddy, S.V. Nair, A.S. Nair, N. Sivakumar, Electrospun α-Fe_2O_3 nanostructures for supercapacitor applications, J. Mater. Chem. A 1 (2013) 11698–11704.

[27] F.L. Lai, Y.E. Miao, Y.P. Huang, T.S. Chung, T.X. Liu, Flexible hybrid membranes of $NiCo_2O_4$-doped carbon nanofiber@MnO_2 core-sheath nanostructures for high-performance supercapacitors, J. Phys. Chem. C 119 (2015) 13442–13450.

[28] W.S. Hummers, R.E. Offeman, Preparation of graphitic oxide, J. Am. Chem. Soc. 80 (1958) 1339–1339.

[29] X.H. Qin, Structure and property of electrospinning PAN nanofibers by different preoxidation temperature, J. Therm. Anal. Calorim. 99 (2010) 571–575.

[30] S.B. Ye, J.C. Feng, P.Y. Wu, Deposition of three-dimensional graphene aerogel on nickel foam as a binder-free supercapacitor electrode, ACS Appl. Mater. Interfaces 5 (2013) 7122–7129.

[31] Q.J. Duan, B. Wang, H.P. Wang, Effects of stabilization temperature on structures and properties of polyacrylonitrile (PAN)-based stabilized electrospun nanofiber mats, J. Macromol. Sci. Part B: Phys. 51 (2012) 2428–2437.

[32] S.S. Ji, Z. Yang, C. Zhang, Z.Y. Liu, W.W. Tjiu, I.Y. Phang, Z. Zhang, J.S. Pan, T.X. Liu, Exfoliated MoS_2 nanosheets as efficient catalysts for electrochemical hydrogen evolution, Electrochim. Acta 109 (2013) 269–275.

[33] X.P. Dai, K.L. Du, Z.Z. Li, H. Sun, Y. Yang, W. Zhang, X. Zhang, Enhanced hydrogen evolution reaction on few-layer MoS_2 nanosheets-coated functionalized carbon nanotubes, Int. J. Hydrogen Energy 40 (2015) 8877–8888.

[34] P.P. Wang, H.Y. Sun, Y.J. Ji, W.H. Li, X. Wang, Three-dimensional assembly of single-layered MoS_2, Adv. Mater. 26 (2014) 964–969.

[35] D.Z. Wang, X.Y. Zhang, Y.L. Shen, Z.Z. Wu, Ni-doped MoS_2 nanoparticles as highly active hydrogen evolution electrocatalysts, RSC Adv. 6 (2016) 16656–16661.

[36] J.F. Xie, J.J. Zhang, S. Li, F. Grote, X.D. Zhang, H. Zhang, R.X. Wang, Y. Lei, B.C. Pan, Y. Xie, Controllable disorder engineering in oxygen-incorporated MoS_2 ultrathin nanosheets for efficient hydrogen evolution, J. Am. Chem. Soc. 135 (2013) 17881–17888.

[37] C.B. Ma, X.Y. Qi, B. Chen, S.Y. Bao, Z.Y. Yin, X.J. Wu, Z.M. Luo, J. Wei, H.L. Zhang, H. Zhang, MoS_2 nanoflower-decorated reduced graphene oxide paper for high-performance hydrogen evolution reaction, Nanoscale 6 (2014) 5624–5629.

[38] Y.P. Huang, Y.E. Miao, L.S. Zhang, W.W. Tjiu, J.S. Pan, T.X. Liu, Synthesis of few-layered MoS_2 nanosheet-coated electrospun SnO_2 nanotube heterostructures for enhanced hydrogen evolution reaction, Nanoscale 6 (2014) 10673–10679.

[39] J.X. Guo, F.F. Li, Y.F. Sun, X. Zhang, L. Tang, Oxygen-incorporated MoS_2 ultrathin nanosheets grown on graphene for efficient electrochemical hydrogen evolution, J. Power Sources 291 (2015) 195–200.

[40] J. Bonde, P.G. Moses, T.F. Jaramillo, J.K. Norskov, I. Chorkendorff, Hydrogen evolution on nano-particulate transition metal sulfides, Faraday Discuss. 140 (2009) 219–231.

[41] J.F. Xie, Y. Xie, Structural engineering of electrocatalysts for the hydrogen evolution reaction: Order or disorder? ChemCatChem 7 (2015) 2568–2580.